Adaptive Stiffness Control of Series Elastic Actuator Manipulators Based on Dynamic System

Kunlin Guo[1], Chao Zeng[2], Weiyong Si[3], Ning Wang[4], and Chenguang Yang[2*]

Abstract— **In traditional control methods, Series Elastic Actuator (SEA) joint manipulators are limited by their hardware and can only perform simple tasks with low stiffness. To address this issue, we propose a stiffness adjustment control strategy for SEA manipulators based on Dynamic Systems (DS) with good generalization performance. By enhancing the generalization capability of DS in complex tasks and combining posture control, the SEA manipulators can autonomously adjust control gains and postures according to task requirements to achieve higher stiffness at the end-effector. Experimental results involving the activation of air switches with different stiffness levels and installation angles have demonstrated the effectiveness of our proposed method. The results indicate that compared to traditional methods of adjusting the control gain and retraining DS for similar tasks, our approach exhibits superior generalization performance while maintaining end-effector stiffness during interactions.**

I. INTRODUCTION

Humans possess highly flexible physical manipulation capabilities, particularly in simultaneously attending to multiple dimensions such as position, stiffness, and safety when performing complex tasks. In recent years, with the increasing presence of robots in people's daily lives [1][2] and the growing number of industrial robots collaborating with humans to perform tasks [3][4], robots need to acquire human-like skills in order to collaborate more effectively with humans.

In [5], researchers proposed a novel learning framework based on Dynamic Movement Primitives (DMPs) is proposed to realize a more complete skill transfer process by considering both location trajectory and stiffness profile. In addition to the DMPs method, [6] proposes an impedance control dynamic system parameter optimization method based on an exponential natural evolution strategy, which enhances the robustness and adaptability of skill learning, thereby ensuring global stability. For the sake of both stability and the accuracy of demonstration learning, [7] proposes a polar space analysis method to derive parameter constraints to ensure the unique minimization of the nerve energy function, and further construct a global asymptotically stable autonomous dynamic system (ADS) with predefined position constraints. Meanwhile, the generalization ability of the learned ADS is quantitatively analyzed by using the flexibility of the nerve energy function. However, these methods exhibit poor generalization performance for training dynamic systems (DS) on tasks with complex trajectories. Additionally, conventional DS methods only consider position, which is insufficient for effective robotic arm control, as it neglects other important factors.

Series Elastic Actuator (SEA) is a new type of robot actuator, which is characterized by the use of flexible components in the drive system [8]. This flexible element is usually a spring or other variable stiffness element, which is used to cushion and absorb the external impact force. Compared with traditional rigidly connected robots, flexible joint robots can better adapt to environmental changes and uncertainties, and have better stability and safety. In [9], researchers designed a low-cost two-degree-of-freedom SEAs series robotic arm that uses SEAs for force sensing to reduce the strain in the rod. Researchers also studied how to reduce the collision force of the robot at the physical level[10], and how to ensure the safety of the SEA robot in the process of interacting with humans by designing a fast response SEA admittance control method[11]. SEAs-based robots have been widely studied and applied in various fields, such as medical treatment, rescue, manufacturing and so on. Despite its certain technical challenges and cost problems, it is still expected to become one of the important technologies robots.

In interactive scenarios, stiffness control topic is also a very important research. In general, the control of the stiffness of the manipulator can be achieved efficiently by adjusting the gain parameters in impedance controllers [5][12]. There are various approaches to designing stiffness gains. [13] uses the extended the Kalman filter (EKF) to estimate the stiffness of the interactive environment and designs an optimal LQR interaction controller based on robot-environment coupled dynamics modeling. This enables the manipulator to interact with the external environment and respond appropriately without force sensors. However, due to the limitation of motor performance, the control of gain on stiffness is limited, especially for SEA joint manipulators. In order to enable the manipulators with low joint stiffness to achieve the task of high stiffness, this paper proposes a novel method that adapts the the end stiffness ellipsoid of the SEA joint robot by combining the control gain and orientation control strategy.

The main contributions of this paper are listed as follows:

1) Drawing on the combination of DMP and rotation-translation matrices for generalization [14], we propose

[1]Key Laboratory of Autonomous Systems and Networked Control, School of Automation Science and Engineering, South China University of Technology, Guangzhou, 510640, China.

[2]Department of Computer Science, University of Liverpool, Liverpool, L69 3BX, UK.

[3] School of Computer Science and Electronic Engineering, University of Essex, Wivenhoe Park, Colchester CO4 3SQ.

[4] Bristol Robotics Laboratory, University of the West of England, Bristol, BS16 1QY, UK.

*Corresponding author, cyang@ieee.org

enhancing the overall generalization performance of DS model by incorporating a rotation matrix.
2) Propose an optimization function for comprehensively considering the overall orientation of the robot arm and comprehensively adjusting joint gain and end pose, to realize the task of achieving higher end stiffness for the robot arm with lower joint stiffness.
3) At the same time, the stiffness does not need to be aligned with DS, only real-time stiffness needs to be collected, and the robot arm can automatically adjust its pose to achieve the required stiffness for task execution

The paper is structured as follows. Section II begins with the presentation of the control theory for SEA manipulators, followed by the generalization performance of DS in complex tasks is improved through the incorporation of the rotation matrix. Subsequently, an optimization function is devised to adaptively adjust the stiffness of the robot arm's end for optimal stiffness control under DS strategy. Section III then validates the efficacy of the proposed method through experiments conducted on a Baxter robot for activating 1P and 2P air switches with the robotic arm.

II. FUNDAMENTALS

A. SEAs dynamics

According to [15], the dynamics of SEAs are given as following:

$$\begin{aligned} \boldsymbol{M}(\boldsymbol{q})\ddot{\boldsymbol{q}} + \boldsymbol{C}(\boldsymbol{q},\dot{\boldsymbol{q}})\dot{\boldsymbol{q}} + \boldsymbol{g}(\boldsymbol{q}) =& \boldsymbol{K}(\boldsymbol{\theta}-\boldsymbol{q}) + \boldsymbol{D}(\dot{\boldsymbol{\theta}}-\dot{\boldsymbol{q}}) \\ &+ \boldsymbol{\tau}_{ext} \\ \boldsymbol{B}\ddot{\boldsymbol{\theta}} + \boldsymbol{K}(\boldsymbol{\theta}-\boldsymbol{q}) + \boldsymbol{D}(\dot{\boldsymbol{\theta}}-\dot{\boldsymbol{q}}) =& \boldsymbol{\tau}_m \end{aligned} \tag{1}$$

where $\boldsymbol{M} \in \mathbb{R}^{n\times n}$, $\boldsymbol{C} \in \mathbb{R}^{n\times n}$ and $\boldsymbol{g} \in \mathbb{R}^{n\times n}$ denote inertia matrix , Coriolis/centrifugal matrix and gravity matrix seperately. $\boldsymbol{K} \in \mathbb{R}^{n\times n}$ and $\boldsymbol{B} \in \mathbb{R}^{n\times n}$ denotes joint stiffness matrix and motor inertia matrix. The motor torques $\boldsymbol{\tau_m}$ clearly correspond to the generalized forces acting on the rotors.

The general model considers the joint damping by $\boldsymbol{D}(\dot{\theta}-\dot{q})$, which could be ignored in common situations besides the passivity situations when using. In order to simplify the control strategy, in this work of paper we would ignore the damping item, so the reduced SEA model would be simplified as following:

$$\begin{aligned} \boldsymbol{M}(\boldsymbol{q})\ddot{\boldsymbol{q}} + \boldsymbol{C}(\boldsymbol{q},\dot{\boldsymbol{q}})\dot{\boldsymbol{q}} + \boldsymbol{g}(\boldsymbol{q}) &= \boldsymbol{K}(\boldsymbol{\theta}-\boldsymbol{q}) + \boldsymbol{\tau}_{ext} \\ \boldsymbol{B}\ddot{\boldsymbol{\theta}} + \boldsymbol{K}(\boldsymbol{\theta}-\boldsymbol{q}) &= \boldsymbol{\tau}_m \end{aligned} \tag{2}$$

Unlike the comprehensive model, the reduced model only exhibits coupling between the dynamics of $\boldsymbol{q}$ and $\boldsymbol{\theta}$ through the joint stiffness. This unique structure can be leveraged for controller design purposes.

B. Learning the DS skill from human

The passive DS controller [16] generates the robot force control command to follow the desired velocity:

$$\begin{aligned} \boldsymbol{F}_c &= \boldsymbol{D}\left(\boldsymbol{x}_r\right)\left(\dot{\boldsymbol{x}}_d - \dot{\boldsymbol{x}}_r\right) \\ \boldsymbol{D}\left(\boldsymbol{x}_r\right) &= Q\left(\boldsymbol{x}_r\right)\Lambda Q\left(\boldsymbol{x}_r\right)^T \end{aligned} \tag{3}$$

In our DS, the desired motion is defined as $\dot{\boldsymbol{x}}_d = \left(\boldsymbol{x}_r\right) + \boldsymbol{f}_n\left(\boldsymbol{x}_r\right)$, where $\boldsymbol{f}\left(\boldsymbol{x}_r\right)$ denotes the desired DS motion and $\boldsymbol{f}_n\left(\boldsymbol{x}_r\right)$ represents the learning-based DS modulation. The basis vectors $\boldsymbol{e}_1, \ldots, \boldsymbol{e}_N$ form an orthonormal set, with $\boldsymbol{e}_1 = \frac{\boldsymbol{f}(\boldsymbol{x}_r)}{\|\boldsymbol{f}(\boldsymbol{x}_r)\|}$ aligning with the desired motion direction. Additionally, $\boldsymbol{e}_2$ is obtained by rotating 90^o around the normal of the moving plane with respect to $\boldsymbol{e}_1$. These basis vectors $\boldsymbol{e}_1, \ldots, \boldsymbol{e}_N$ correspond to the columns of the matrix $\boldsymbol{Q}\left(\boldsymbol{x}_r\right)$. Furthermore, $\boldsymbol{\Lambda}$ is a diagonal matrix containing eigenvalues $\lambda_1, \ldots, \lambda_N$, which characterize the damping properties of a robot controller.

By utilizing the passive DS controller, it becomes possible to specify both the desired velocity and damping parameters, thereby enabling the robot to exhibit the desired performance characteristics. When learning a skill from human demonstrations, the focus is typically on modeling the velocity-position relationship of the demonstrated trajectory. A similar model, resembling Stable Estimators of Dynamical Systems (SEDS) and Locally Active-Globally Stable Dynamical Systems (LAGS-DS), has been introduced in references [17] and [18]. These DS models ensure global asymptotic stability, guaranteeing convergence to the target point. Moreover, to replicate human motion effectively, they not only generate velocities based on the robot's state but also rapidly replan trajectories to adapt to changing task conditions, as discussed in references [19] and [20].

1) Learning the DS Motion Model From Human: To enhance the precision of extracting features from human activation of the air switch, we partition the entire activation task into three distinct phases, illustrated in Fig.1. In this figure, the black star denotes the initial position, and the three red lines correspond to each of these phases.

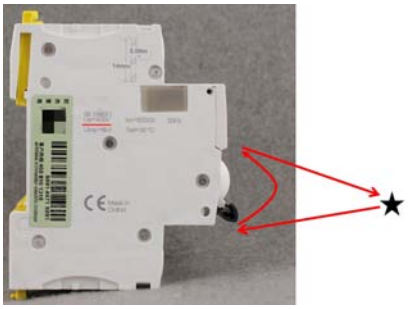

Fig. 1: Three phases of manipulator activating air switch task.

1) Phase 1: The end-effector will continuously approach the air switch until it reaches the activation position of the air switch.
2) Phase 2: The end-effector will activate the air switch.
3) Phase 3: The end-effector will finish the activating and go back to the beginning position for the next task.

Through the analysis of the three phases in Fig.1, we can find that phase 1 and phase 2 are more difficult, especially phase 2, which requires the end of the robot arm to perform the task with a nonlinear stroke that fits the air switch with appropriate stiffness, so as to realize the complex task of activating the air switch.

In phase 1 of the task, the robot needs to handle the uncertainty associated with the position of the contact surface and effectively control the interaction force during penetration. This implies that the robot should be able to adapt its motion and force application to successfully overcome the initial resistance and establish contact with the target surface.

In phase 2, the goal is to activate the air switch. In order to achieve this, the robot must maintain contact with the air switch, ensure that it maintains proper contact, and apply the necessary force in the vertical direction to push the switch. In the following chapters, the stiffness adjustment method proposed in this paper will be introduced, so that the manipulator can obtain the required interactive stiffness during the task.

A unified Dynamical Systems (DS) model is proposed to encompass the entire motion process. This comprehensive model aims to ensure both the generalization performance of the model and its ability to perform effectively in the face of disturbances. By consolidating the various aspects of the motion process into a single model, the proposed unified DS model facilitates a more cohesive and robust approach to motion control, enabling the system to adapt to different conditions while maintaining overall quality of performance.

2) Coupled DS model: The model presented in our study distinguishes itself from other motion models in dynamic systems (DS) by integrating three interconnected DS models, namely DS1, DS2, and DS3, each aligned with distinct phases of the task. These models are trained using demonstration data segmented by task phases. During phase 1, DS1 is employed either to approach the activation position of the air switch or to return the system to its initial point following a disturbance. DS1 incorporates a mobile attractor guided by a virtual dynamic system, facilitating precise control over the robot's movements during these crucial phases. DS2 is dedicated to phase 2 and is responsible for executing the activating motion required for the air switch. This model focuses on guiding the robot's actions during the activating phase to ensure effective and accurate performance. DS3 serves a specific function of moving the end-effector back to the beginning position once the cutting task is completed. This phase is crucial for resetting the system and preparing it for subsequent tasks or operations. By incorporating these three coupled DS models, each tailored to a specific phase of the task, our approach aims to provide a comprehensive and adaptive framework for controlling the robot's motion throughout the entire process. In DS1's scenario, a dynamic system model is configured along the cutting direction. DS1 initiates upon DS2 achieving its target position. The robot's positional data is transformed into the state vector $\boldsymbol{x}_r$, and DS1's output $\dot{\boldsymbol{x}}_1 \in \mathbb{R}^3$directs the robot's velocity commands.

$$\begin{cases} \dot{\boldsymbol{x}}_1 = \boldsymbol{f}_{DS1}\left(\boldsymbol{x}_r\right) = \boldsymbol{A}_1 \cdot \boldsymbol{x}_r + \boldsymbol{b}_1 \\ \boldsymbol{x}_r^* = \boldsymbol{A}_1^{-1} \cdot \boldsymbol{b}_1 \end{cases} \tag{4}$$

where $\boldsymbol{A}_1 \in \mathbb{R}^{3\times3}$ represents diagonal matrices with negative gains, and $\boldsymbol{b}_1 \in \mathbb{R}^3$ is computed upon reaching the target point $\boldsymbol{x}_r^*$.

For the task of activating the air switch, the air switch might not be completely fixed vertically, such as horizontal. For multi-stage DS coupled tasks, we propose an adjustment method to adapt to the change of task target pose. The multi-stage DS coupling task can generally be divided into three DSs, the first DS for close to the task starting position, the second DS for specific execution, and the third DS for return. In this method, we believe that the first DS and the second DS do not need to be adjusted, and the task can be completed by adjusting the DS of the second task according to the change of the task target pose. To this end, in this paper, we improve on the basis of (5) :

$$\begin{cases} \dot{\boldsymbol{x}}_1 = \boldsymbol{f}_{DS1}\left(\boldsymbol{x}_r\right) = \boldsymbol{R} \cdot \left(\boldsymbol{A}_1 \cdot \boldsymbol{x}_r + \boldsymbol{b}_1\right) \\ \boldsymbol{x}_r^* = \boldsymbol{A}_1^{-1} \cdot \boldsymbol{b}_1 \end{cases} \tag{5}$$

where $\boldsymbol{R} \in \mathbb{R}^{3\times3}$ represents a translation matrix, which rotates the DS2 to the rotation angle of the air switch by taking the target position of DS1, that is, the starting point of the air switch task, as the circle center.

In phase 3, the motion direction points away from the tissue, ensuring that DS3 guides the end-effector back to its initial position upon completion of the activation task. DS3, denoted as $\dot{\boldsymbol{\xi}}_d = \boldsymbol{f}_{DS3}\left(\boldsymbol{\xi}_1\right) = \boldsymbol{A}_3 \cdot \boldsymbol{\xi}_1 + \boldsymbol{b}_3\left(\xi_1^*\right)$ (similar to DS2), activates only after DS1 has reached its target point. Due to the interdependency among the DS models introduced here, $\boldsymbol{f}_{DS1}$, $\boldsymbol{f}_{DS2}$, and $\boldsymbol{f}_{DS3}$ collectively form $\boldsymbol{f}_{coupleDS}$.

C. Dynamic System Stiffness-adaptive GMM/GMR

In contrast to the conventional approach of modifying stiffness and task control for manipulator arms, the joints of the Baxter manipulator employed in this investigation are equipped with series elastic actuators (SEA) characterized by low joint stiffness. Consequently, it is imperative to fine-tune the orientation of the end-effector to augment the overall stiffness and proficiently perform tasks necessitating elevated stiffness levels.

It is imperative to conduct a comprehensive analysis of the demonstration trajectories by considering multiple observations. Our proposed approach entails the selection of a set of H reference points within the task environment. Subsequently, we employ a transformation technique to map the demonstrations from the base coordinate system to the coordinates associated with these reference points, employing the following method:

$$\boldsymbol{X}^{(r)} = \boldsymbol{R}^{(r)^{-1}}\left(\boldsymbol{X} - \boldsymbol{d}^{(r)}\right),\ \boldsymbol{K}_h^{(r)} = \boldsymbol{R}^{(r)^T}\boldsymbol{K}_h\boldsymbol{R}^{(r)} \tag{6}$$

In this context, the position vector $\boldsymbol{X} \in \mathbb{R}^{m\times1}$ and the stiffness of the human arm endpoint $\boldsymbol{K}_h \in \mathbb{R}^{n\times n}$ are

combined to create the data point $\boldsymbol{Y} = [\boldsymbol{X}; vec(\boldsymbol{K})]$, where $vec(\cdot)$ represents a vectorization operation [21]. The subscript r denotes the r-th reference point, with $\boldsymbol{R}^{(r)}$ and $\boldsymbol{d}^{(r)}$ representing the rotation matrix and translation vector of the r-th reference point relative to the base coordinates, respectively.

Thus, drawing inspiration from the work [22], the formulated Dynamic System Stiffness-adaptive GMM (DSS-GMM) in the coordinate system of the r-th reference point can be expressed as:

$$p\left(\boldsymbol{Y}^{(r)}\right) = \sum_{n=1}^{N} \pi_n^{(r)} \mathcal{N}\left(\boldsymbol{Y}^{(r)} | \boldsymbol{\mu}_n^{(r)}, \boldsymbol{\Sigma}_n^{(r)}\right) \tag{7}$$

where $\pi \in [0, 1]$ is the prior weighting and $\mathcal{N}$ is the amount of Gaussian models which were given as follows:

$$\mathcal{N}\left(\boldsymbol{Y} | \boldsymbol{\mu}, \boldsymbol{\Sigma}\right) = \frac{1}{\sqrt{(2\pi)^L |\boldsymbol{\Sigma}|}} e^{-\frac{1}{2} Log_{\boldsymbol{\mu}}(\boldsymbol{Y}) \boldsymbol{\Sigma}^{-1} Log_{\boldsymbol{\mu}}(\boldsymbol{Y})} \tag{8}$$

where $L = m + n + n\left(n-1\right)/2$, $\boldsymbol{\mu}$ and $\boldsymbol{\Sigma}$ are the center and covariance matrix of the Gaussian model.

Furthermore, the parameters in equation (8) can be estimated through the Expectation–Maximization algorithm [23], specifically developed to maximize the log-likelihood function outlined in equation (7). It is crucial to emphasize that the DSS-GMM methodology autonomously learns its parameters for different reference points, resulting in the derivation of H distinct sets of parameters.

In the course of DS tasks, the DSS-GMR framework is employed to reproduce the sequence of robot stiffness by leveraging the DSS-GMM model. Diverging from the conventional practice of employing time as the input parameter, we choose to utilize the position of the robot arm's end-effector denoted as $\boldsymbol{X}_I$ as the input variable. This approach allows the reproduced stiffness to adapt dynamically based on user interactions, rather than being solely dependent on temporal progression. Consequently, the reproduced data, along with its center and covariance, can be represented as:

$$\boldsymbol{Y} = \begin{bmatrix} \boldsymbol{X}_I \\ vec\left(\boldsymbol{K}_O\right) \end{bmatrix}, \boldsymbol{\mu} = \begin{bmatrix} \boldsymbol{\mu}_I \\ \boldsymbol{\mu}_O \end{bmatrix}, \boldsymbol{\Sigma} = \begin{bmatrix} \boldsymbol{\Sigma}_{II} & \boldsymbol{\Sigma}_{IO} \\ \boldsymbol{\Sigma}_{OI} & \boldsymbol{\Sigma}_{OO} \end{bmatrix} \tag{9}$$

where $\boldsymbol{K}_O$ as the output is the stiffness of the robot arm's end-effector. The DSS-GMR in the coordinate system of the r-th reference point is formulated as follows:

$$p\left(\boldsymbol{K}_O^{(r)} | \boldsymbol{X}_I^{(r)}\right) = \sum_{n=1}^{N} h_n^{(r)} \mathcal{N}\left(\hat{\boldsymbol{\mu}}_n^{(r)}, \hat{\boldsymbol{\Sigma}}_n^{(r)}\right) \tag{10}$$

with

$$h_n^{(r)} = \frac{\pi_n^{(r)} \mathcal{N}\left(\boldsymbol{X}_I^{(r)} | \boldsymbol{\mu}_{I,n}^{(r)}, \boldsymbol{\Sigma}_{II,n}^{(r)}\right)}{\sum_{j=1}^{N} \pi_j^{(r)} \mathcal{N}\left(\boldsymbol{X}_I^{(r)} | \boldsymbol{\mu}_{I,n}^{(r)}, \boldsymbol{\Sigma}_{II,n}^{(r)}\right)} \tag{11}$$

$$\boldsymbol{\Phi}_n^{(r)} = \log_{\hat{\boldsymbol{\mu}}_O^{(r)}}\left(\hat{\boldsymbol{\mu}}_{O,n}^{(r)}\right) + \bar{\boldsymbol{\Sigma}}_{OI,n}^{(r)} \bar{\boldsymbol{\Sigma}}_{II,n}^{(r)^{-1}} \log_{\boldsymbol{X}_I^{(r)}}\left(\boldsymbol{\mu}_{I,n}^{(r)}\right) \tag{12}$$

$$\boldsymbol{K}_O^{(r)} = \hat{\boldsymbol{\mu}}_O^{(r)} \leftarrow \exp_{\hat{\boldsymbol{\mu}}_O^{(r)}}\left(\sum_{n=1}^{N} h_n^{(r)} \boldsymbol{\Phi}_n^{(r)}\right) \tag{13}$$

$$\begin{aligned} \boldsymbol{W}^{(r)} = \hat{\boldsymbol{\Sigma}}_{OO}^{(r)} = \sum_{n=1}^{N} h_n^{(r)} \Big(& \bar{\boldsymbol{\Sigma}}_{OO,n}^{(r)} - \bar{\boldsymbol{\Sigma}}_{OI,n}^{(r)} \bar{\boldsymbol{\Sigma}}_{II,n}^{(r)^{-1}} \\ & + \boldsymbol{\Phi}_n^{(r)} \boldsymbol{\Phi}_n^{(r)^T} \Big) - \boldsymbol{K}_O^{(r)} \boldsymbol{K}_O^{(r)^T} \end{aligned} \tag{14}$$

where the symbol $\hat{\boldsymbol{\Sigma}}$ indicates the parallel transform operation $\Gamma_{\boldsymbol{\mu}_O \to \hat{\boldsymbol{\mu}}_O}\left(\Sigma\right)$ in common with (4).

To transform the calculated reproduced stiffness matrices obtained from equation (13) to the base coordinates, the inverse operation of equation (6) is applied in the following manner:

$$\boldsymbol{K}_{OB}^{(r)} = \boldsymbol{R}^{(r)} \alpha \boldsymbol{K}_O^{(r)} \boldsymbol{R}^{(r)^T} \tag{15}$$

where α is the user-defned positive parameter to scale the stiffness for adapting to the task environment.

Referring to the weighted Karcher mean algorithm in [18], an actual stiffness that fused all $\boldsymbol{K}_{OB}^{(r)}, r = 1, 2, \ldots, H$, is iteratively computed until convergence

$$\boldsymbol{K}_e \leftarrow \boldsymbol{K}_e^{\frac{1}{2}} \exp\left(\sum_{r=1}^{H} \omega_r \log\left(\boldsymbol{K}_e^{-\frac{1}{2}} \boldsymbol{K}_{OB}^{(r)} \boldsymbol{K}_e^{-\frac{1}{2}}\right)\right) \boldsymbol{K}_e^{\frac{1}{2}} \tag{16}$$

with

$$\omega_r = \frac{tr\left(\boldsymbol{W}^{(r)^{-1}}\right)}{\Sigma_{t=1}^{H} tr\left(\boldsymbol{W}^{(r)^{-1}}\right)} \tag{17}$$

which implies that the weight allocated to the covariance matrix of the reference point in equation (16) rises as the trace value decreases.

In this study, the demonstration data $\boldsymbol{Y}$ is obtained using MYO armbands and a Microsoft Kinect sensor. Assuming the hand and forearm of the human subject are stationary, the MYO armband, equipped with surface Electromyography (sEMG) sensors and an Inertial Measurement Unit (IMU), can capture muscle activations and determine the orientation of the human arm endpoint. Consequently, the stiffness of the human arm endpoint $\boldsymbol{K}_h$ can be computed based on these signals and the inherent constant stiffness of the human subject (for further details, refer to [14]). Additionally, the position of the human arm endpoint $\boldsymbol{X}$ can be detected using the Kinect device.

To simplified the calculation, in this paper, the scale factor α is set as 1, and due to the physical limitation and safety concern, the stiffness of manipulator joints are restricted as follows:

$$\begin{aligned} \boldsymbol{K}_{jr} &= \boldsymbol{J}^T \boldsymbol{K}_e \boldsymbol{J} \\ \boldsymbol{K}_j &= \boldsymbol{K}_{j_{min}} + \frac{\left(\boldsymbol{K}_{jr} - \boldsymbol{K}_{j_{min}}\right)^2}{\boldsymbol{K}_{j_{max}} - \boldsymbol{K}_{j_{min}}} \end{aligned} \tag{18}$$

where $\boldsymbol{J}$ is the Jacobian matrix of manipulator arm, $\boldsymbol{K}_j$ is the restricted joint stiffness of the robot arm, $\boldsymbol{K}_{jr}$ is the Jacobian without stiffness restrict, $\boldsymbol{K}_{j_{min}}$ and $\boldsymbol{K}_{j_{max}}$ are the prescribed minimum and maximum stiffness respectively.

In order to obtain greater stiffness at the end of the manipulator, the common method is to increase the gain of the controller. However, for Baxter manipulator whose SEA constitutes joint, there is an upper limit of joint stiffness. Simply increasing controller gain may not always achieve the desired stiffness. To do this, we use the following approach to balance the choice between attitude and gain:

$$\begin{aligned} \min\ & \frac{1}{2}\boldsymbol{O}_e^T \alpha_1 \cdot \boldsymbol{O}_e + \alpha_2 \left(\boldsymbol{K}_d - \boldsymbol{K}_j\right) \\ s.t.\ & \alpha_1 + \alpha_2 = 1 \\ & \boldsymbol{O}_e = \boldsymbol{O}_r - \boldsymbol{O} \\ & \boldsymbol{K}_{jr} = \boldsymbol{J}\left(\boldsymbol{q}\right)^T \boldsymbol{K}_e \boldsymbol{J}\left(\boldsymbol{q}\right) \\ & \boldsymbol{K}_j = \boldsymbol{K}_{j_{min}} + \frac{\left(\boldsymbol{K}_{jr} - \boldsymbol{K}_{j_{min}}\right)^2}{\boldsymbol{K}_{j_{max}} - \boldsymbol{K}_{j_{min}}} \end{aligned} \tag{19}$$

where α_1 and α_2 represent the weight parameters between controller gain and poseture adjustment, respectively, $\boldsymbol{O}$, $\boldsymbol{O}_r$ and $\boldsymbol{O}_e$ represents the orientation of the end effectior, the desired orientation and their difference respectively. Through the above methods, we can obtain the optimal posture $\boldsymbol{O}_d$ of the end of the manipulator with the desired stiffness.

D. Dynamic System Stiffness-adaptive SEA Controller

According to [15], where a Controller Design Based on the Cascaded Structure was given, combined with the DS and stiffness posture proposed in this paper, we can obtain the controller with variable stiffness for SEA manipulator:

$$\begin{aligned} \boldsymbol{\tau}_m =& \boldsymbol{\tau}_d + \boldsymbol{B}\boldsymbol{K}^{-1}\left(\boldsymbol{D}_\tau\left(\dot{\boldsymbol{\tau}}_d - \dot{\boldsymbol{\tau}}\right) + \boldsymbol{K}_\tau\left(\boldsymbol{\tau}_d - \boldsymbol{\tau}\right)\right) + \boldsymbol{B}\ddot{\boldsymbol{q}} \\ \boldsymbol{\tau}_d =& \boldsymbol{g}\left(\boldsymbol{q}\right) + \boldsymbol{J}\left(\boldsymbol{q}\right)^T\left(\boldsymbol{\Lambda}\left(\boldsymbol{x}\right)\ddot{\boldsymbol{x}}_d + \boldsymbol{\mu}\left(\boldsymbol{x}, \dot{\boldsymbol{x}}\right)\dot{\boldsymbol{x}}_d \right. \\ & \left. - \boldsymbol{K}_d\tilde{\boldsymbol{x}} - \boldsymbol{D}_d\dot{\tilde{\boldsymbol{x}}}\right) \\ \boldsymbol{K}_d =& \boldsymbol{K}_j \\ \boldsymbol{D}_d =& \boldsymbol{D}_d = \eta\sqrt{\boldsymbol{K}_d} \\ \boldsymbol{\Lambda}\left(\boldsymbol{x}\right)\ddot{\boldsymbol{x}}_d + \boldsymbol{\mu}_c\left(\boldsymbol{x}, \dot{\boldsymbol{x}}\right)\dot{\boldsymbol{x}}_d =& \boldsymbol{F}_c + \boldsymbol{F}_e \\ \boldsymbol{F}_e =& \boldsymbol{J}\cdot\boldsymbol{\tau}_{ext} \\ \boldsymbol{F}_c =& \boldsymbol{J}\cdot\boldsymbol{\tau}_m \end{aligned} \tag{20}$$

where $\boldsymbol{\tau}$ is joint torque, $\boldsymbol{K}_d$ and $\boldsymbol{K}_d$ are again the symmetric and positive definite matrices of the desired stiffness and damping. $\boldsymbol{\Lambda}\left(\boldsymbol{x}\right)$ is the cartesian inertia matrix and $\boldsymbol{\mu}_c\left(\boldsymbol{x}, \dot{\boldsymbol{x}}\right)$ is the cartesian corresponding Coriolis/centrifugal matrix with $\tilde{\boldsymbol{x}} = \boldsymbol{x} - \boldsymbol{x}_d$, $\boldsymbol{\tau} = \boldsymbol{K}\left(\boldsymbol{\theta} - \boldsymbol{q}\right)$, $\ddot{\boldsymbol{\theta}} = \boldsymbol{K}^{-1}\ddot{\boldsymbol{\tau}} + \ddot{\boldsymbol{q}}$. The stability of this controller could be proof with similar type of [15], which is proved with asymptotic stability.

III. EXPERIMENTS

To validate the proposed stiffness control strategy, a Baxter robot with SEA joints is employed in this study to perform the task of activating air switches. By utilizing air switches with varying stiffness levels and mounting angle, the efficacy and generalization performance of the proposed stiffness control strategy are verified.

A. Experiment Results

In the experiment, a 3D motion tracking system composed of a binocular camera and a positioning board as shown in Fig. 2 is employed to capture the trajectory of the demonstrator when activating the air switch. The stiffness information during the activation of the air switch by the demonstrator is acquired using the MYO armband. Finally, during the execution of the task by the Baxter robotic arm, the position and mounting angle of the air switch are determined using a Kinect camera.

(a) Binocular camera (b) Multiple movable targets

Fig. 2: 3D motion tracking system.

There are 8 groups of data collected during demonstrations. As shown in Fig.3, the demonstration is obtained through kinesthetic teaching. At the same time, the operator wears a MYO armband on the upper arm to obtain arm stiffness information. The air switch activate task is divided into three phases, approach, activation and leave. The envelope profiles of the filtered EMG signals are shown in Fig.4a, from which we can see that the maximum stiffness values of 20-25 Nm are required to complete this task, and the different operation habits of different trainers caused different displacement and speed in the x and z directions. Based on the end-effector position of the robotic arm obtained through the 3D motion tracking system as shown in Fig.4, we derived the end-effector dynamic system (DS) required for activating the air switch as illustrated in Fig.5.

Fig. 3: A human operator demonstrates the task through kinesthetic teaching.

In this experiment, the Baxter robot uses a traditional force-coupled DS strategy to activate the 1P air switch, as

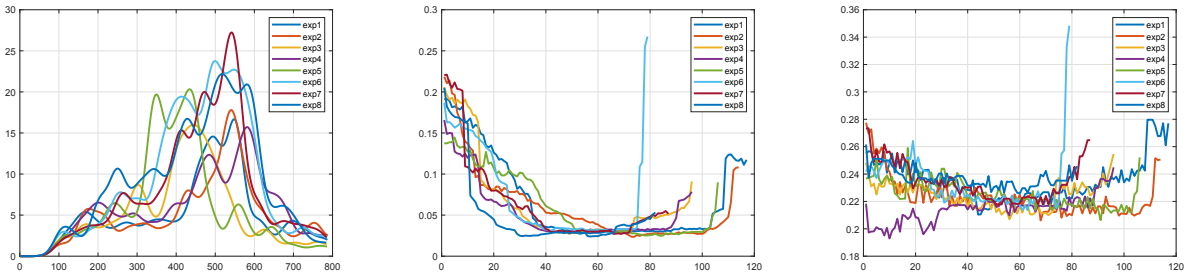

(a) Arm stiffness signals obtained in demonstrations.

(b) Position in x direction.

(c) Position in z direction.

Fig. 4: Human demonstration data.

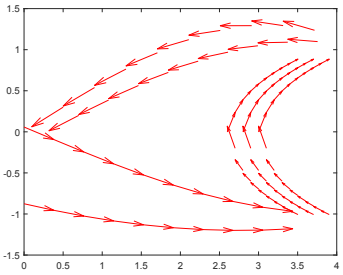

Fig. 5: Red lines represent the generated DS with the target air switch on the right side.

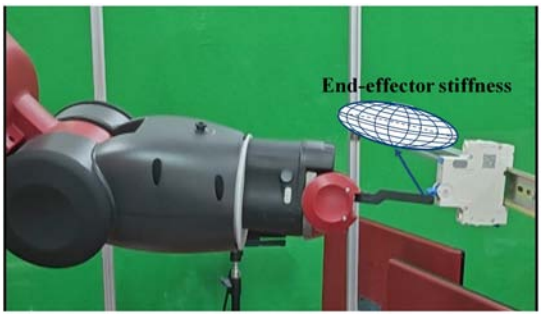

Fig. 6: The stucking position with the traditional DS to activate the 1P air switch and the end-effector stiffness ellipsoid.

shown in Fig.6. In this process, the end-effector of baxter would be stuck by the air switch. The reason is that Baxter is a SEA joint manipulator, whose joint stiffness is not large enough in most cases. The traditional force-coupled DS strategy only considers the expected position, the stiffness information is not addressed which is required in this contact task.

In accordance with Baxter's official joint stiffness specifications, the stiffness values of the three joints adjacent to the end-effector are all 15 Nm. However, this value is insufficient to generate the required force for actuating the air switch, due to the highly non-linear stiffness characteristics of the system. This presents a significant challenge for conventional DS strategies.

The end stiffness ellipsoid of the manipulator arm is shown in Fig.6, which is the experiment of Baxter using the traditional method to activate airswitch. By this strategy as we can see, the end-effector is using the minor axis of the stiffness ellipsoid to activate air switch which requires higher stiffness. In this case, the manipulator could not accomplish the task of 1P air switch. Therefore, we introduced an innovative DS control strategy, and the experimental process is shown in Fig.7, which can be viewed in the video. By using our strategy, the posture of the SEA matipulator could be adaptively adjusted to gain the desired high stiffness at the end-effector, eventually successfully activate both 1P and 2P air switches as shown in Fig.7 and Fig.8.

Fig. 7: The robot successfully complete the 1p air switch task using the proposed method.

Fig. 8: The robot successfully complete the 2P air switch task using the proposed method.

As shown in Figt.9, in this experiment, the position of air switch is not changed while the mounting angle is changed. Due to the changes in the pose of the task object, the trajectory required to perform the task has also been altered. Typically, when using traditional DS strategies, it is necessary to retrain and obtain new DS to accommodate

Fig. 9: The robot successfully complete the task using the proposed method without retraining the DS.

such variations in the task. However, by enhancing the generalization performance of the DS strategy and integrating an optimization function for stiffness control, this study demonstrates the capability to accomplish the task without the need for retraining the DS.

IV. CONCLUSIONS

In this paper, we propose a stiffness adjustment control strategy for SEA manipulators based on DS with better generalization performance. By enhancing the generalization capability of DS in complex tasks and combining posture control in SEA manipulator, the SEA manipulator can autonomously adjust control gain and posture according to task requirement to achieve higher stiffness at the end-effector. Experimental results involving the activation of air switches with different stiffness levels and installation angles have demonstrated that our method exhibits better generalization performance while maintaining higher end-effector stiffness compared to traditional methods of adjusting control gain. However, in our work, the DS only considers the position of the robotic arm end-effector without considering its orientation. In future work, we plan to incorporate both position and orientation in the DS to achieve better control effectiveness for the manipulator.

REFERENCES

[1] M. R. Pedersen, L. Nalpantidis, R. S. Andersen, C. Schou, S. Bøgh, V. Krüger, and O. Madsen, "Robot skills for manufacturing: From concept to industrial deployment," *Robotics and Computer-Integrated Manufacturing*, vol. 37, pp. 282–291, 2016.

[2] F. Stulp and O. Sigaud, "Robot skill learning: From reinforcement learning to evolution strategies," *Paladyn, Journal of Behavioral Robotics*, vol. 4, no. 1, pp. 49–61, 2013.

[3] M. Valori, A. Scibilia, I. Fassi, J. Saenz, R. Behrens, S. Herbster, C. Bidard, E. Lucet, A. Magisson, L. Schaake, J. Bessler, G. B. Prange-Lasonder, M. Kühnrich, A. B. Lassen, and K. Nielsen, "Validating safety in human–robot collaboration: Standards and new perspectives," *Robotics*, vol. 10, no. 2, 2021.

[4] P. Adami, P. B. Rodrigues, P. J. Woods, B. Becerik-Gerber, L. Soibelman, Y. Copur-Gencturk, and G. Lucas, "Effectiveness of vr-based training on improving construction workers' knowledge, skills, and safety behavior in robotic teleoperation," *Advanced Engineering Informatics*, vol. 50, p. 101431, 2021.

[5] C. Yang, C. Zeng, C. Fang, W. He, and Z. Li, "A dmps-based framework for robot learning and generalization of humanlike variable impedance skills," *IEEE/ASME Transactions on Mechatronics*, vol. 23, no. 3, pp. 1193–1203, 2018.

[6] Y. Hu, G. Chen, Z. Li, and A. Knoll, "Robot policy improvement with natural evolution strategies for stable nonlinear dynamical system," *IEEE Transactions on Cybernetics*, vol. 53, no. 6, pp. 4002–4014, 2023.

[7] Z. Jin, W. Si, A. Liu, W.-A. Zhang, L. Yu, and C. Yang, "Learning a flexible neural energy function with a unique minimum for globally stable and accurate demonstration learning," *IEEE Transactions on Robotics*, vol. 39, no. 6, pp. 4520–4538, 2023.

[8] G. Pratt and M. Williamson, "Series elastic actuators," in *Proceedings 1995 IEEE/RSJ International Conference on Intelligent Robots and Systems. Human Robot Interaction and Cooperative Robots*, vol. 1, pp. 399–406 vol.1, 1995.

[9] E. Campbell, Z. C. Kong, W. Hered, A. J. Lynch, M. K. O'Malley, and J. McLurkin, "Design of a low-cost series elastic actuator for multi-robot manipulation," in *2011 IEEE International Conference on Robotics and Automation*, pp. 5395–5400, 2011.

[10] P. Wang, Q. Zhu, X. Hu, J. Wu, and R. Xiong, "Research on interaction safety of human-robot collision based on series elastic actuator," in *2018 5th International Conference on Information, Cybernetics, and Computational Social Systems (ICCSS)*, pp. 180–185, 2018.

[11] H. Zhong, X. Li, L. Gao, and C. Li, "Toward safe human–robot interaction: A fast- response admittance control method for series elastic actuator," *IEEE Transactions on Automation Science and Engineering*, vol. 19, no. 2, pp. 919–932, 2022.

[12] L. Liu, S. Leonhardt, C. Ngo, and B. J. E. Misgeld, "Impedance-controlled variable stiffness actuator for lower limb robot applications," *IEEE Transactions on Automation Science and Engineering*, vol. 17, no. 2, pp. 991–1004, 2020.

[13] L. Roveda, A. A. Shahid, N. Iannacci, and D. Piga, "Sensorless optimal interaction control exploiting environment stiffness estimation," *IEEE Transactions on Control Systems Technology*, vol. 30, no. 1, pp. 218–233, 2022.

[14] C. Yang, C. Zeng, P. Liang, Z. Li, R. Li, and C.-Y. Su, "Interface design of a physical human–robot interaction system for human impedance adaptive skill transfer," *IEEE Transactions on Automation Science and Engineering*, vol. 15, no. 1, pp. 329–340, 2018.

[15] C. Ott, *Cartesian impedance control of redundant and flexible-joint robots*. Springer, 2008.

[16] K. Kronander and A. Billard, "Passive interaction control with dynamical systems," *IEEE Robotics and Automation Letters*, vol. 1, no. 1, pp. 106–113, 2016.

[17] S. M. Khansari-Zadeh and A. Billard, "Learning stable nonlinear dynamical systems with gaussian mixture models," *IEEE Transactions on Robotics*, vol. 27, no. 5, pp. 943–957, 2011.

[18] N. Figueroa and A. Billard, "Locally active globally stable dynamical systems: Theory, learning, and experiments," *The International Journal of Robotics Research*, vol. 41, no. 3, pp. 312–347, 2022.

[19] S. S. Mirrazavi Salehian, M. Khoramshahi, and A. Billard, "A dynamical system approach for catching softly a flying object: Theory and experiment," *IEEE Transactions on Robotics*, vol. 32, no. 2, pp. 10. 462–471, 2016.

[20] S. S. M. Salehian and A. Billard, "A dynamical-system-based approach for controlling robotic manipulators during noncontact/contact transitions," *IEEE Robotics and Automation Letters*, vol. 3, no. 4, pp. 2738–2745, 2018.

[21] J. Mandel, "Generalisation de la theorie de plasticite de w. t. koiter," *International Journal of Solids and Structures*, vol. 1, no. 3, pp. 273–295, 1965.

[22] N. Jaquier, L. Rozo, D. G. Caldwell, and S. Calinon, "Geometry-aware manipulability learning, tracking, and transfer," *The International Journal of Robotics Research*, vol. 40, no. 2-3, pp. 624–650, 2021. PMID: 33994629.

[23] T. Moon, "The expectation-maximization algorithm," *IEEE Signal Processing Magazine*, vol. 13, no. 6, pp. 47–60, 1996.